Monolithic Resonant-Cantilever-Based CMOS Microsystem for Biochemical Sensing

Yue Li, Cyril Vancura, Kay-Uwe Kirstein, *Member, IEEE*, Jan Lichtenberg, and Andreas Hierlemann, *Member, IEEE*

***Abstract*—A resonant cantilever-based microsystem aimed at biochemical sensing is presented. The sensor system comprises a magnetically actuated resonant cantilever sensor array integrated with the feedback circuitry, digital control circuitry and a serial interface on a single chip in 0.8 μm CMOS technology. The sensor system shows a frequency stability of better than 3 Hz in water corresponding to a detection limit of about 30 pg mass loading. The system has been used for the detection of antibody-antigen interaction on the cantilever surface. The possibility to actuate and operate cantilever arrays in a liquid environment opens up a variety of new applications for bio-chemical sensing.**

***Index Terms*—Biosensor, chemical sensor, CMOS, liquid phase, monolithic integration, resonant cantilever.**

I. Introduction

MASS-SENSITIVE sensors based on resonant microcantilevers have been developed by various groups [2]–[12]. The resonance frequency of a cantilever beam is dependent on its total mass. A mass change due to adsorption/desorption of analyte molecules in a sensitive layer on the cantilever can, therefore, be measured by monitoring the change of its resonance frequency. Due to their high sensitivity (e.g., absolute mass sensitivity reported in the attogram range in the gas phase [8], [9]) cantilever systems constitute promising mass-sensitive transducers for chemical and biological sensing [2]–[12]. In most cases, resonant cantilevers have been used for detection in the gas phase [1], [5]–[9], [11].

In contrast to physisorption-type interaction in the gas-phase, mass-sensitive biosensors in the liquid phase rely on biomolecular, interaction such as antigen-antibody binding. These interactions are usually highly specific and, therefore, sometimes referred to as molecular recognition processes. When a cantilever is operated in liquid phase, both, the cantilever resonance frequency and its quality factor Q drop due to massive damping losses: liquids feature a much larger viscosity than gases. Especially the drop in the quality factor as a consequence of the liquid damping reduces the frequency stability and, consequently, the overall sensor resolution, if no counter-measures are taken [3]. The damping losses can be addressed by monolithic integration of a feedback circuitry with a dedicated signal amplification stage on the sensor chip hosting the cantilevers. In other cantilever implementations, external components have been used to excite the cantilever or to realize the feedback loop [10], [12]). The work presented here focuses on the development of the CMOS-integrated circuitry of a magnetically actuated, self-oscillating cantilever sensor system that features four cantilevers for highly stable operation in liquid phase. The system is intended to serve biochemical sensor applications. The cantilevers themselves, their magnetic actuation scheme, and their liquid-phase characterization as well as biosensor measurements have been previously presented [3]–[6], [20].

In the next sections, we will present the design of the cantilever array sensor system and its circuitry components (Fig. 1). The system has been fabricated in 0.8-μm 2M 2P CMOS (Complementary Metal Oxide Semiconductor) technology as available from *austria**micro**systems*, Graz, Austria. Dedicated post-CMOS micromachining enabled the integration of circuitry and micromechanical transducers on the same substrate.

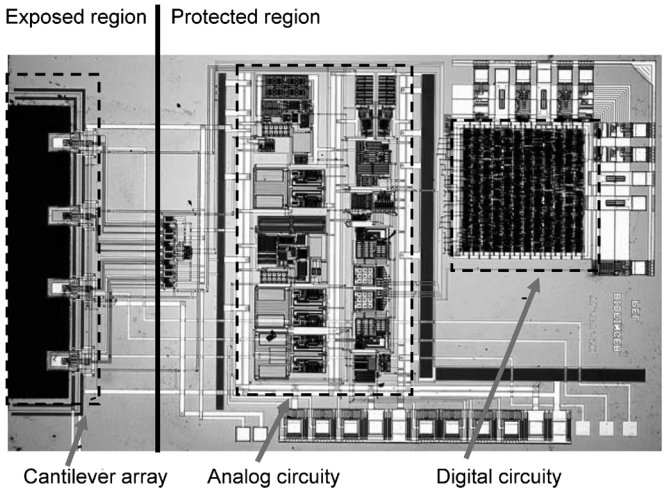

Fig. 1. Micrograph of the resonant cantilever biosensor system.

II. System Description

The sensor system includes four cantilevers that are monolithically integrated with dedicated analog and digital circuitry

Manuscript received December 4, 2006; revised August 14, 2007. First published April 18, 2008; current version published October 29, 2008. This work was supported in part by the Swiss Federal Office of Science and Education within the EU project "Biofinger" (IST-2001-34544). This paper was recommended by Associate Editor A. G. Andreou.

Y. Li was with the Physical Electronics Laboratory, ETH Zurich, 8092 Zurich, Switzerland. He is now with the CSEM, Zurich CH-8006, Switzerland.

C. Vancura was with the Physical Electronics Laboratory, ETH Zurich, 8092 Zurich, Switzerland. He is now with the Robert Bosch Corporation, Palo Alto, CA 94304 USA.

K.-U. Kirstein was with the Physical Electronics Laboratory, ETH Zurich, 8092 Zurich, Switzerland. He is now with Uster Technologies AG, 8610 Uster, Switzerland (e-mail: kirstein@miromico.ch).

J. Lichtenberg was with the Physical Electronics Laboratory, ETH Zurich, 8092 Zurich, Switzerland. He is now with the Hocoma AG, 8008 Zurich, Switzerland.

A. Hierlemann is with the Bio Engineering Laboratory, Department of Biosystems Science and Engineering (BSSE), ETH Zurich, 4058 Basel, Switzerland.

Digital Object Identifier 10.1109/TCSI.2008.922027

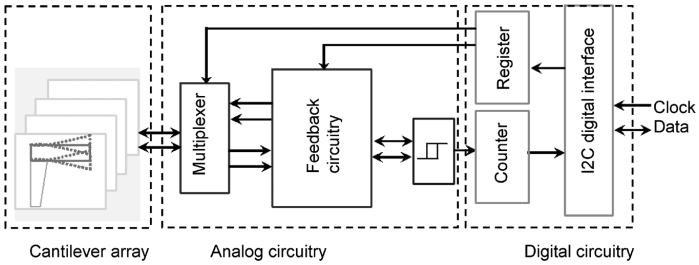

Fig. 2. Architecture of the resonant cantilever array microsystem for biochemical sensing.

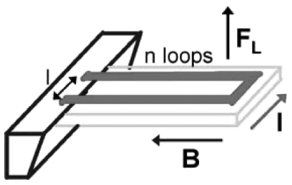

Fig. 3. Schematic and cross section of the magnetically actuated resonant cantilever.

as shown in Fig. 2. The system allows for biochemical measurements using three biochemically functionalized cantilevers as sensor cantilevers while having one uncoated cantilever as a reference element. The cantilever array has a common feedback circuit and a common frequency readout circuitry accessible through an analog multiplexer. A 16-bit configuration register, a 24-bit counter and the serial interface (I^2C) are included in the digital part of the circuitry.

A single cantilever is activated at a time by switching it to the feedback circuitry, and, then, the oscillation frequency is measured. This process is sequentially applied to the four cantilevers. The start-up of the oscillation needs less than 1 ms, but the frequency has to be counted at least during 1 second gate time to obtain the desired frequency precision in the range of 1 Hz. It takes about 5 s in total to measure all cantilevers. Fortunately, this measurement time is acceptable, as the system dynamics are in the range of more than 15 min, determined by the binding process of the biomolecular samples. Therefore, the feedback circuitry can be shared for the four cantilevers which allows for a significant reduction in the overall chip area.

III. Resonant Cantilever Design

A. Electromagnetic Actuation

An electromagnetic actuation scheme has been chosen to excite the cantilever structure in a liquid environment. The working principle of the electromagnetic excitation is based on the Lorentz force as illustrated in Fig. 3. An oscillation of the cantilever can be achieved by generating a periodic force. Three elements are required to generate the Lorentz force: a current, a coil, and a constant magnetic field. The coil is realized as metal loops integrated along the edges of the cantilever. An external magnetic field oriented in parallel to the cantilever axis is provided, e.g., by a small permanent magnet [6].

An electric current through the coil then produces a Lorentz force perpendicular to the surface of the chip. By applying an AC current of suitable frequency to the current loops a mechanical oscillation of the cantilever can be achieved. The Lorentz

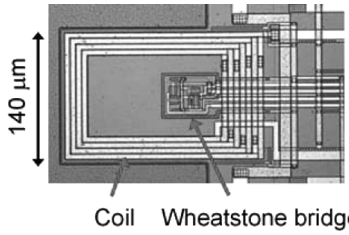

Fig. 4. Micrograph of the magnetically actuated resonant cantilever.

force, F_{Lorentz}, acting on the cantilever, oriented perpendicularly to the cantilever plane, can be approximated by the following equation[5]:

$$F_{\mathrm{Lorentz}} = n_{\mathrm{coil}} \cdot I_{\mathrm{coil}} \cdot l_{\mathrm{coil}} \cdot B_{\mathrm{external}}. \tag{1}$$

Here, I_{coil} represents the current through the coil, l_{coil} the mean length of the coil loop perpendicular to the external magnetic field, B_{external}, and n_{coil} denotes the number of coil loops. Upon applying a sinusoidal electrical current to the coil, a sinusoidal Lorentz-force is generated, which produces a harmonic out-of-plane oscillation of the cantilever. Fig. 4 shows the micrograph of a resonant cantilever.

The resonance frequency of the cantilever is determined by the natural frequency of the cantilever structure and the viscoelastic damping through the liquid environment. While the natural frequency is governed by the geometry and mechanical properties of the cantilever structure, the damping can be represented as an additional mass-loading of the cantilever.

The mechanical properties of the CMOS-layer materials are defined for a given CMOS process, however, the cantilever geometry (length and width) can be selected to achieve a certain target resonant frequency in the liquid phase. The length and width of the cantilever are 150 μm and 140 μm. The target frequency here amounts to several hundred kHz to reach the necessary sensor resolution and to yield, at the same time, signal bandwidths that do not lead to an excessive power dissipation with respect to the used CMOS-technology.

By using the two metallization layers of the used CMOS-process a coil of 8 windings ($n_{\mathrm{coil}} = 8$) has been realized along the cantilever edges.

B. Vibration Detection

The cantilever vibration is detected by a piezoresistive Wheatstone bridge integrated on the cantilever as shown in Fig. 4. The Wheatstone bridge consists of four diode-connected pMOS transistors.

The piezoresistive effect in slightly doped silicon can be described as a relative resistance change, $\Delta R/R$

$$\frac{\Delta R}{R} = \pi_L \sigma_L + \pi_T \sigma_T \tag{2}$$

where $\pi_{L,T}$ are the longitudinal and transversal piezoresistive coefficients, and $\sigma_{L,T}$ denote the respective stress-components. The piezoresistive coefficients in parallel and perpendicular orientation with respect to the cantilever axis have opposite signs. Therefore, a differential signal can be obtained by arranging two resistors in parallel and two resistors perpendicularly to the cantilever axis in a Wheatstone-bridge configuration (see Fig. 5). The common-mode voltage varies only by a few percent, since

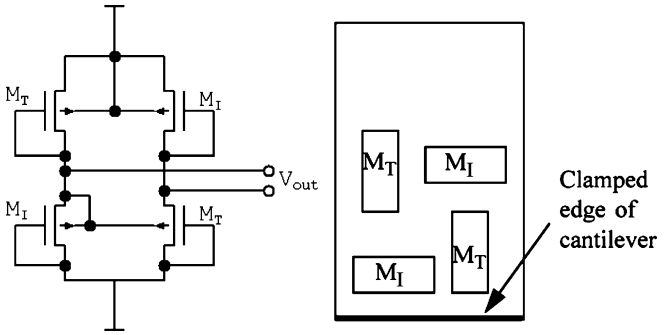

Fig. 5. Schematic of the PMOS-transistor Wheatstone bridge to detect the vibration of the cantilevers. The bridge is supplied with 5 Volts and the transistor W/L ratio is 9 μm/3 μm.

the absolute values of the longitudinal and transversal piezoresistive coefficients are almost identical [7].

In comparison to a Wheatstone bridge consisting of diffused resistors (resistive load less than 1 kΩ), the transistor configuration as described above consumes less area and features a higher resistive load (about 20 kΩ). This lowers the power dissipation on the cantilever, which is a crucial point for chemical as well as for biological sensing applications, as heating might significantly change the sensitivity of the absorption or binding process [6].

As a positive side-effect the matching of the used PMOS-transistors is better than that of minimum-size diffused resistors, leading to a lower offset voltage at the differential bridge output. The Wheatstone bridge is located at the clamped edge of the cantilever, where the mechanical stress is maximal, so that a large piezoresistive output signal can be achieved.

C. Post-CMOS Micromachining

The device presented in this paper has been fabricated in a modified industrial CMOS process in combination with post-CMOS micromachining. After completion of the CMOS processing, the cantilevers were released by two post-processing steps that are conducted on wafer level. First, silicon membranes were formed by anisotropic wet etching (KOH) of the bulk silicon substrate. To ensure a defined membrane thickness, an electrochemical etch-stop technique was used so that the etching stops at the n-well of the CMOS process. Thereafter, the cantilevers were released by reactive-ion etching (RIE) from the wafer front side.

IV. Feedback Circuitry Design

A. Feedback Circuitry Architecture

The self-oscillation of the resonant cantilever is obtained by connecting it to the on-chip feedback loop. The main task of the feedback circuitry includes starting up and maintaining the cantilever oscillation with the oscillation frequency being close to the fundamental resonance frequency. The design specifications result from possible applications, desired cantilever performance and package requirements.

Fig. 6 shows a block diagram of the complete feedback electronics. The circuitry consists of two amplifier stages, one programmable phase shifter to meet the oscillation condition, and an amplitude regulator to maintain a stable oscillation. High-pass filters after each amplification stage are aimed at removing the DC-offset and the flicker noise introduced by the Wheatstone bridge and the amplification stages. A class-AB buffer is added as the last stage to drive the low-resistance coil, whose load impedance is in the range of 50 Ω. The oscillation frequency is measured by means of a 24-bit digital counter, which can be either gated by a dedicated command over the serial interface (I2C), or, if higher precision is required, by an external gating input. The counter value can be read-out via the serial interface, which also can be used to define the microsystem configuration. In the following, the circuitry implementation and the electrical characterization results of the key building blocks, including the gain stages, the phase shifter and the amplitude regulator, will be detailed.

B. Gain Stages

The vibration-induced differential output signal of the Wheatstone bridge exhibits an amplitude of 1 mV for a bias-current of about 8 mA (corresponding to an excitation voltage of 400 mV) and a magnetic field generated by a 100-mT electromagnet. Consequently, the feedback circuitry has to provide an amplification of at least 60 dB for a cantilever operation in liquid to achieve an overall loop gain of more than 0 dB.

The maximum offset generated by the Wheatstone bridge is about 25 mV. In order to avoid the saturation of the amplifier, two gain stages with an additional high-pass filter were implemented to obtain the target gain of more than 60 dB for stable operation.

A further requirement is that the gain should be adjustable in the range of 10 dB, since the fabrication spread of the cantilever properties reaches maximally 10%. Overall, the gain stages consist of an instrumentation amplifier with a fixed gain of 30 dB and a variable-gain amplifier providing a gain between 30 dB and 40 dB. In order to maximize the possible voltage signal swing and to lower the sensitivity to external interferences, the complete feedback signal path has been designed in a fully-differential configuration as shown in Fig. 6.

The realization of the differential instrumentation amplifier by conventional two-, three-, or four-opamp readout circuits would require a combination of amplifiers that consumes comparably much power and chip area. The differential difference amplifier (DDA) featuring two differential inputs and only one differential output stage is very attractive, since it needs less power and chip area. For that reason, a DDA topology was used for both amplifiers [13].

The schematic of the instrumentation amplifier is shown in Fig. 7. Two inputs are connected to the feedback network, and the other two inputs can be connected to the output of the Wheatstone bridge. The closed-loop gain is defined by the feedback resistors as shown in (3), where $R_1 = 200\ \Omega$ and $R_2 = 6\ \mathrm{k}\Omega$

$$A_{CL} = 1 + \frac{R_2}{R_1}. \tag{3}$$

The simplified schematic of the differential difference amplifier is depicted in Fig. 8. The circuit is based on a folded-cascode transconductance amplifier with two differential input stages and one differential Miller output stage [14]. The necessary

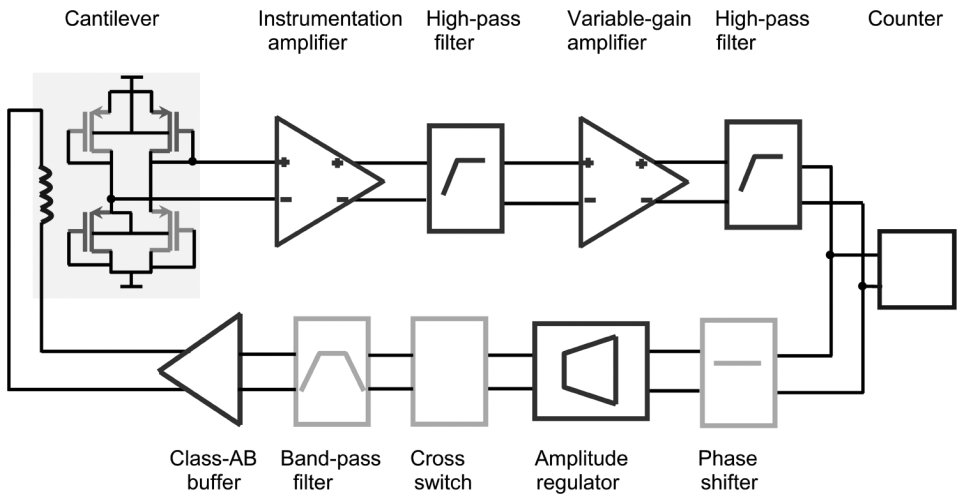

Fig. 6. Block diagram of the fully differential feedback circuitry.

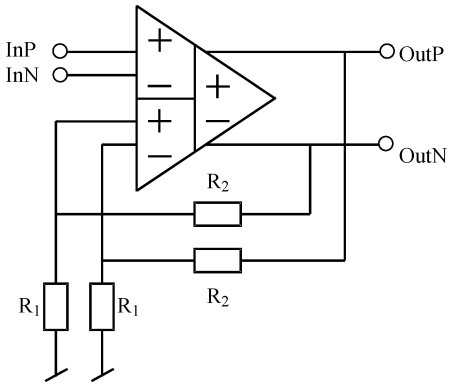

Fig. 7. Schematic representation of a differential instrumentation amplifier based on a DDA topology.

gain-bandwidth product (GBW) is given by the resonance frequency of the cantilever of 250 kHz (in liquid environment), which has a variation of 20 kHz, and a closed-loop gain of 30 dB, and is set to 10 MHz to preserve a design margin.

The main task of the second amplification stage is to supply the gain required to achieve oscillation conditions. Due to fabrication process variations the cantilevers may show slightly different physical characteristics. The parameters, such as resonance frequency, quality factor, amplitude and phase response at resonance frequency may vary up to 10%. In particular, the amplitude response is strongly dependent on the magnetic field, the cantilever fabrication spread and the operation environment, which is here the liquid phase. A variable-gain amplifier is, therefore, an essential element to deal with possible variations and to have a flexible system.

The topology of the variable-gain amplifier is depicted in Fig. 9 [15] and includes a linear transconductance cell [16], [17] on the feedback loop of a non-inverting amplifier. Considering a linear transconductor featuring a transconductance, G_{mg}, and two identical resistors, R_g, in the feedback network, the relationship described in the following equation is obtained:

$$\begin{aligned} V_{od} &= \frac{1}{R_g G_{mg}} V_{id} = \frac{1}{G_d} V_{id}, \\ V_{od} &= V_{OutP} - V_{OutN}, \\ V_{id} &= V_{InP2} - V_{InN2}. \end{aligned} \tag{4}$$

If the linear feedback transconductance, G_{mg}, can be tuned by an external voltage or current, then a variable-gain differential output instrumentation amplifier has been realized. In order to avoid an external tunable voltage source, the tunable current source, I_v, was implemented in this design, since a programmable current source can be easily realized. The current source, I_g, has been set set to a constant current, and I_v is tunable. The DDA of this amplifier stage is realized by the same architecture as the first amplifier stage (see Fig. 8), but has been optimized for a higher gain-bandwidth product of about 300 MHz, in order to feature a maximum gain of 40 dB.

C. Phase Tuning

The total phase shift generated in the feedback loop partly determines the final oscillation frequency and plays the most important role with regard to the frequency stability. The cantilever as a mechanical resonator should feature a phase response of -90° at the resonance frequency. Due to the low-pass filter function resulting from the Wheatstone bridge and parasitic capacitances, a phase response of -100° was measured. Furthermore, the amplifiers generate additional phase shifts. The system should oscillate as close as possible to the mechanical fundamental cantilever resonance frequency to achieve maximum frequency stability. For this reason, a pseudo-differential first-order all-pass filter, functioning as a phase shifter, was inserted after the amplification stages (see Fig. 10). Its function includes the phase adjustment at different frequencies without changing the amplitude. Its phase response, described in the following equation, was derived from the transfer function

$$\varphi(\omega) = (-2) \cdot \arctan(\omega \cdot R \cdot C) \tag{5}$$

$$R = R_a + R_b || G_{DS}. \tag{6}$$

By switching on different capacitors, the phase can be adjusted. The switches can be set through the I2C interface. To achieve a more accurate phase tuning, an all-pass filter with a transistor, connected in series with the main resistor, has been realized. Varying the gate voltage, V_g, of the transistor allows for a smaller step size in a narrow range.

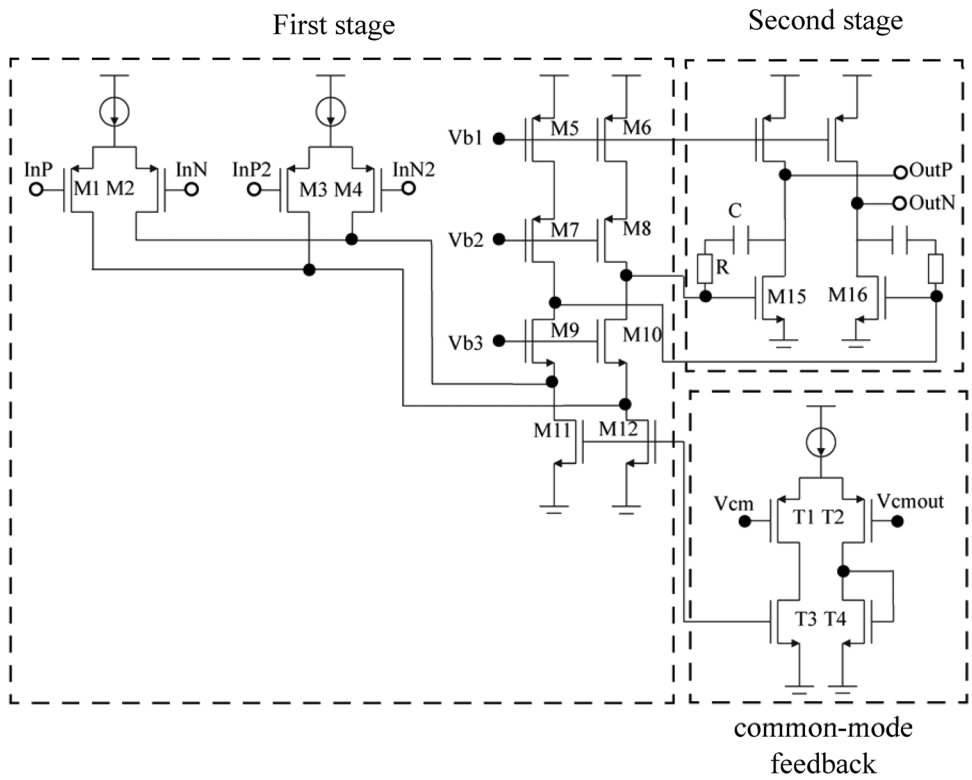

Fig. 8. Schematic of the differential difference amplifier including two stages and a common-mode feedback circuitry. The first stage is based on a folded-cascode transconductance amplifier. The second stage is a differential Miller output stage.

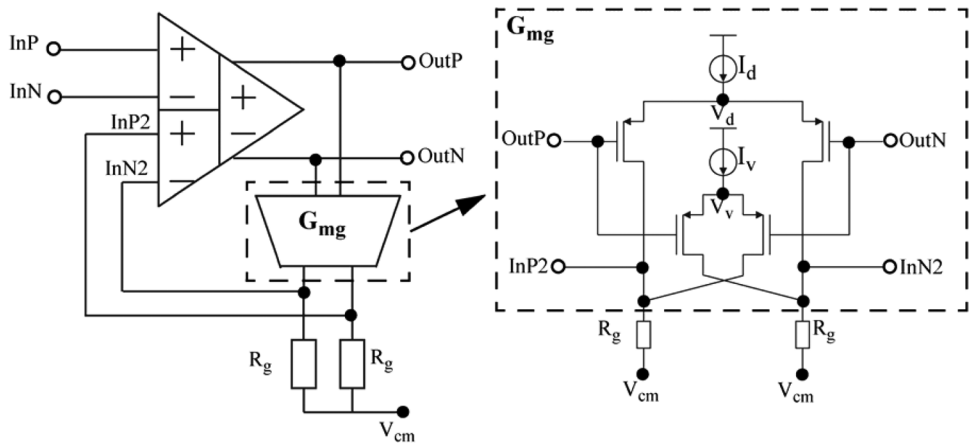

Fig. 9. Schematic of the variable-gain amplifier and the nonlinear transconductance configuration.

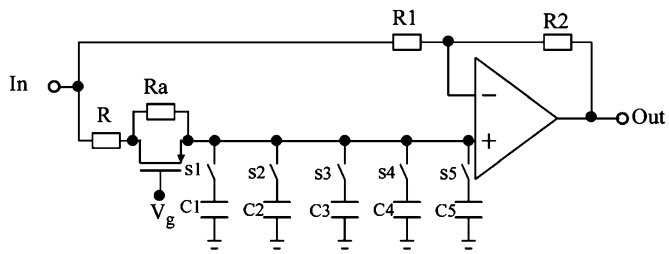

Fig. 10. Block diagram of the all-pass filter used as a phase shifter. Only one branch of the pseudo-differential configuration is shown.

D. Amplitude Regulation

The gain stages and the phase shifter facilitate the initiation of the oscillation. Without any limitation in the gain, the oscillation amplitude will continuously increase until the amplifiers are saturated, which will cause large distortions and, therefore, obstruct a proper frequency measurement. To obtain a stable oscillation, the oscillation amplitude is regulated via a nonlinear transconductance stage, whose amplification factor is dependent on the amplitude of the input signal. Fig. 11 shows the simplified schematic of this amplitude regulator. By combining a simple differential input stage and a linearized differential input stage, the desired characteristics have been achieved.

The first differential pair of Fig. 11 shows the transfer characteristics of a transconductance stage without any linearization, so that a saturation of the output current occurs at a certain input level. The second differential pair is linearized by additional source degradation transistors [18], [19]. By exchanging the dif-

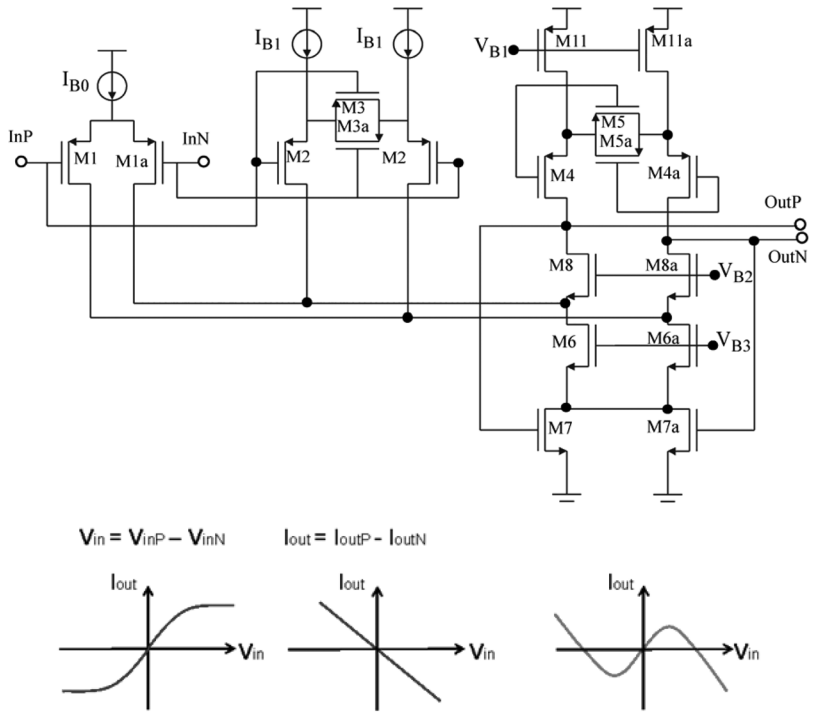

Fig. 11. Simplified schematic of a nonlinear transconductance used as amplitude regulator.

ferential input connections, transfer characteristics with opposite sign and with smaller slope, compared to the first differential pair, can be obtained. By adding up the output currents of these 2 transconductance stages transfer characteristics as shown in the right part of Fig. 11 are realized. The nonlinear transconductance is fully differential and is operated in an open-loop configuration. The overall transconductance of the input stages is small, because it consists of the difference of two transconductances. For this reason, a folded-cascode output stage was employed to achieve a maximum voltage gain of 10 for small input voltages. The transistor dimensions and biasing currents have been designed for an oscillation amplitude of about 350 mV, which determines the position of the peak in the transfer characteristics. The overall gain variation ranges from 1 dB up to 20 dB. For this fully differential configuration without feedback network, a common-mode feedback circuitry based on linear MOS transistors was chosen [19]. The common-mode voltage has been regulated to 2.5 Volt.

E. Class-AB Buffer

The last element in the feedback loop is an output amplifier to drive the signal in the coil featuring a resistance of approximately 50 Ω. The output amplifier must be capable of providing sufficient output current to the coil. A straightforward approach to increase the current driving capability includes to simply increase the bias current in the output stage. However, the power consumption will also be dramatically increased. Efficiency and possible distortion are the two most important parameters to assess the performance of the output amplifier. Some architectures feature good efficiency, but also generate considerable distortions. Considering the resistance of the coil and the power consumption restriction in this stage, a class-AB buffer was chosen,

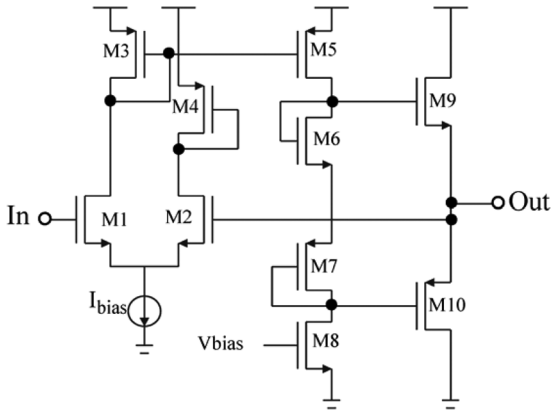

Fig. 12. Schematic of the class-AB buffer. A pseudo-differential architecture has been used in the feedback loop.

which is shown in Fig. 12. A differential signal path has been realized by placing two of these buffers in a pseudo-differential configuration.

F. Frequency Readout and Digital Interface

A straightforward way to monitor the resonance frequency through a digital interface is to convert the oscillation signal into a digital signal, and to then measure the frequency by means of a digital counter. In order to be insensitive to signal offset and noise, a comparator with hysteresis was implemented to convert the differential signal of the feedback circuitry to a digital clock signal of the same frequency (Fig. 2).

The digital core provides the means to control the operation mode of the system via the I2C serial interface bus, and allows for reading out the frequency of the cantilever oscillator via the

same interface. The frequency of the cantilever oscillator is measured using a 24-bit period counter, which operates in two different modes, depending on how the frequency reference is provided.

Alternatively, the output of the comparator can be directly measured using external equipment, which is suitable for testing purposes. The digital counter can be operated in the gated mode and in the triggered mode. In the gated mode, an external time signal is provided to the core. The counter provides the ratio of the cantilever period and the gate time period. The gate time should be at least 1 s in order to provide sufficient measurement accuracy.

In the triggered mode, the I2C read-out command is used to measure the time. The counter provides the number of cantilever oscillation periods between two successive readout commands. If the external device, a microcontroller or an FPGA that issues the read-out command, can be timed and triggered precisely, the counter provides the cantilever frequency in Hz.

The comparison of the two modes shows, that the gated mode is easier to implement and more reliable. A 16-bit control register is available for the system configuration, which includes the selection of the cantilever, the change in the polarity of the feedback signal, and the setting of the delay of the phase shifter.

G. Chip Floor Plan and Packaging

A micrograph of the monolithically integrated cantilever array microsystem is shown in Fig. 1. The floor plan does not only take electronic issues into account, such as analog and digital crosstalk, but is also determined by the packaging approach. For the biochemical application, the sensor part has to be exposed to liquid environment. As a consequence, one of the key issues in designing the chip layout is that the sensing area is accessible to the liquid, while electrical interconnections and circuitry must be kept "dry" at any time. A straightforward solution is to separate the sensor area from the circuitry area and, especially, from the electrical bond contacts.

The packaging requires a distance of more than 1 mm between the exposed region and the protected region. One wide metal line with contact to the substrate is inserted between the sensing area and the analog circuitry to inhibit the diffusion of water through the chip. Additional metal lines have been placed between the analog circuitry and the digital circuitry to eliminate electrical interference by the digital clocks.

The packaging design is shown in Fig. 13. and has been used for the experiments described in the next section. The integrated sensor is attached to a ceramic holder at the bottom of the flow cell, and the flow-through sensor chamber is formed in a PMMA (poly(methylmethacrylate)) block. The necessary permanent magnet can also be placed in the PMMA block. For liquid handling, an external pumping system is used.

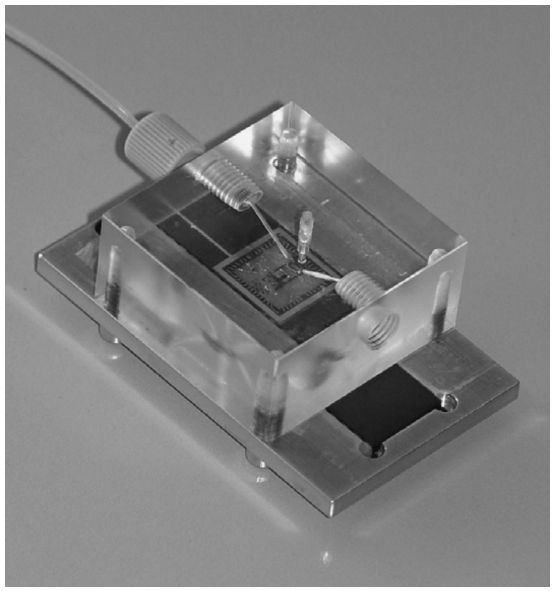

Fig. 13. Photo of the packaged sensor in a flow-through cell.

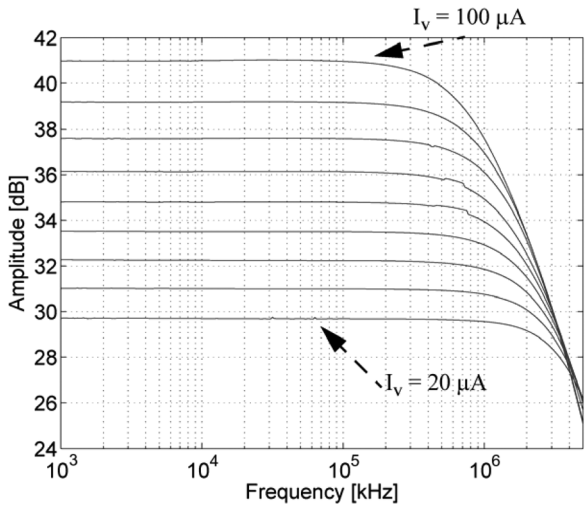

Fig. 14. Measured amplitude response of a variable-gain amplifier upon tuning the current, I_v.

V. Experimental Results

A. Electrical Measurements

1) VGA Characterization: A test structure was designed and integrated on the same die, so that the variable-gain amplifier could be separately characterized. The measured closed-loop transfer function (Fig. 14) shows an adjustable gain between 30 dB and 45 dB via tuning a single bias current. The measured thermal noise of this amplifier is 12 $\mathrm{nV}/\sqrt{\mathrm{Hz}}$ and the 1/f-corner frequency is around 100 Hz.

2) All-Pass Filter: The all-pass filter was separately characterized as well. The measured transfer function is shown in Fig. 15. By switching on different capacitors, the phase can be adjusted at a step size of 5°. The measurements show, that the total tunable range amounts to almost 90°.

3) Sensor System: The final version of the chip has been characterized only in closed-loop configuration, since the feedback loop is directly closed on the chip to avoid the noise coupling from the testing PCB and other equipment. To obtain precise data on the performance of the oscillator, the measurements were carried out in a homogeneous magnetic field. The cantilever was oscillating in water. Fig. 16 shows the measured spectra of the oscillator at different locations of the feedback loop, which were recorded by a spectrum analyzer (Agilent Technologies HP4195). The spectrum of the signal

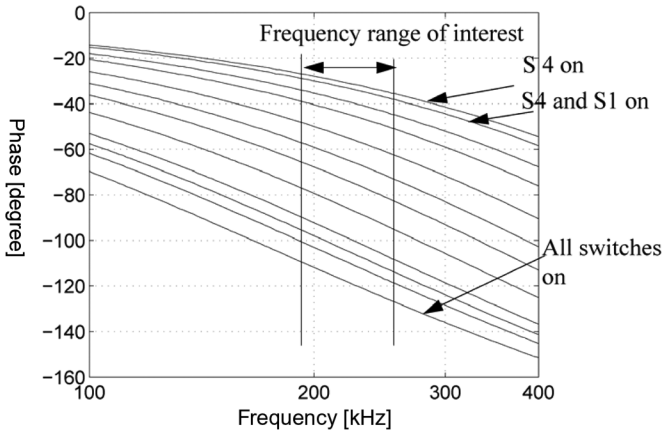

Fig. 15. The measured all-pass filter phase response.

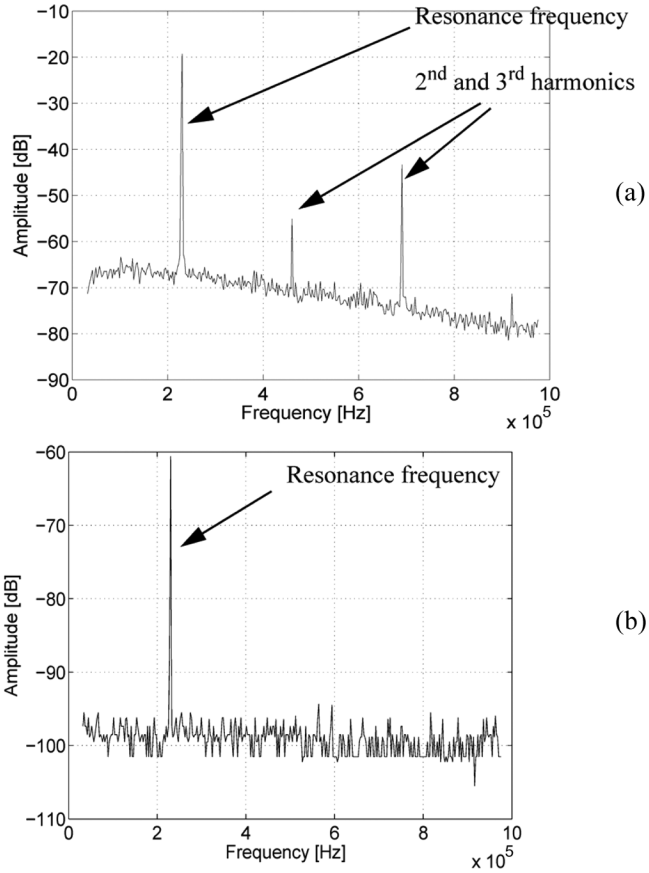

Fig. 16. Spectrum of the cantilever oscillation in water: (a) at the output of the nonlinear transconductance, (b) at the output of the first amplifier. The magnetic field strength was 150 mT, and the gain of the variable gain amplifier has been set to 30 dB.

after the amplitude regulator clearly shows the second and third harmonics as a consequence of the nonlinearity [Fig. 16(a)]. Fortunately, the harmonics have almost disappeared at the output of the cantilever, as can be seen in the spectrum of the output of the first amplification stage [Fig. 16(b)]. This is a consequence of the sharp filter function of the resonator, although the open-loop quality factor of the cantilever structure is only 20 in water. The measurement also shows that the nonlinear transconductance is an efficient amplitude regulator with a simple structure. If thermal or capacitive coupling in the system would exist, the harmonics would directly couple into the input of the feedback circuitry and, thus, reduce the frequency stability of the oscillation. This is one of the reasons, that an electromagnetic excitation was implemented in this system instead of a thermal excitation.

The short-term stability of the oscillator was characterized using the Allan variance. Using a measurement interval of 1 second, the best Allan variance was determined to be $9 \cdot 10^{-6}$. This corresponds to a short-term frequency stability of 1.6 Hz. The best value of the Allan variance of the cantilever oscillator operated in air is two orders of magnitude smaller. The importance of the phase tuning is evident from the measurement results presented in Fig. 17. The phase shift represents the calculated total phase shift in the feedback loop. In this measurement the optimal operation point is located at a phase shift of -50°, where a frequency stability of 1.6 Hz has been achieved. It should be noted, that this optimal operation point depends on the phase response of the cantilever and the resonance frequency. This is the main drawback of the system. Therefore, it is proposed to develop an automated phase tracking technique so that the operating point is always kept at the optimum location.

The whole system including the sensor array, the analog circuitry, and the digital circuitry consumes a total current of 12.5 mA at a supply voltage of 5 Volts, with the major consumers being the two amplification stages.

B. Biochemical Measurements

The device has been extensively tested in liquid phase using polymeric coatings and organic volatiles; the respective procedures and experimental details have been described earlier [20]. The presented cantilever sensor system has additionally been used in label-free biological detection experiments. The binding of prostate-specific antigen (PSA) to antiPSA was chosen as a model assay. PSA is a tumor marker for prostate cancer. This assay has already been successfully used to detect various PSA concentrations [2]. Fig. 18 shows the differential frequency shift (coated cantilever versus uncoated reference cantilever) of the sensor system for three different concentrations of PSA at clinically significant levels. The packaged chips were first cleaned with NaOH and HCl for 1 minute. Thereafter, the chip has been rinsed with de-ionized water and ethanol. The functionalization of the cantilevers was done by immersing one cantilever in a protein-A solution, which works as a linker molecule and by immersing it afterwards in an antiPSA solution. The chips were rinsed with de-ionized water and phosphate-buffered saline (PBS) in between and after the functionalization steps. Then, the functionalized packaged chip was mounted in the fluidic setup, and the experiment was conducted under stopped-flow conditions (no flow during cantilever measurements) applying a flow rate of 10 $\mu\mathrm{L/min}$ to change the analyte concentrations in the measurement chamber. As can been seen in Fig. 18, the cantilevers show a distinct response to all three PSA concentrations, and PSA concentrations of 10 ng/mL in phosphate-buffered saline (PBS) could be detected. The measurements were all performed with the same device, which was regenerated with NaOH and HCl after each step. For more details on the experimental procedure, see [20]. The

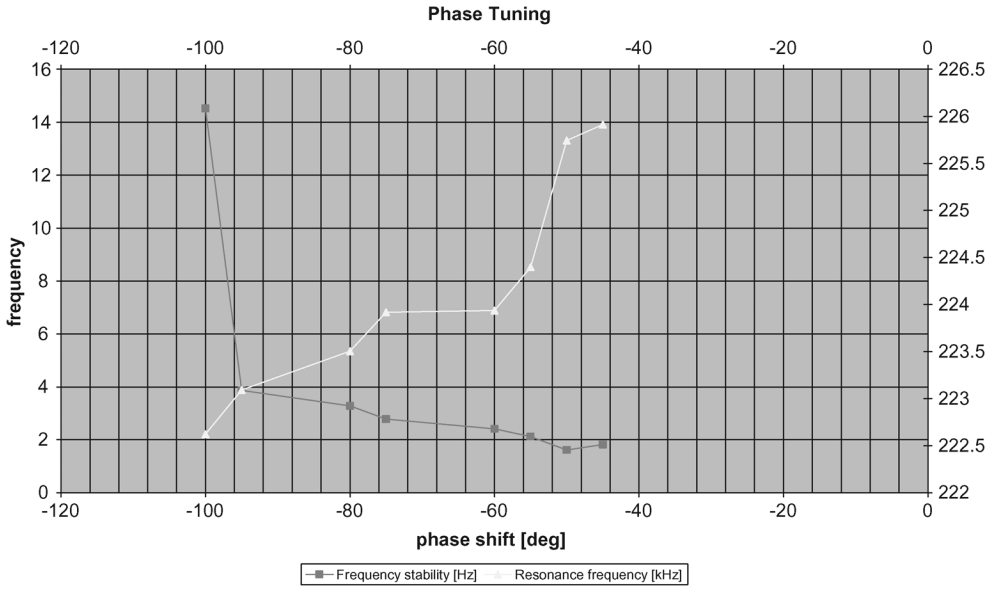

Fig. 17. Influence of the programmable phase shift on resonance frequency (right axis) and frequency stability (left axis).

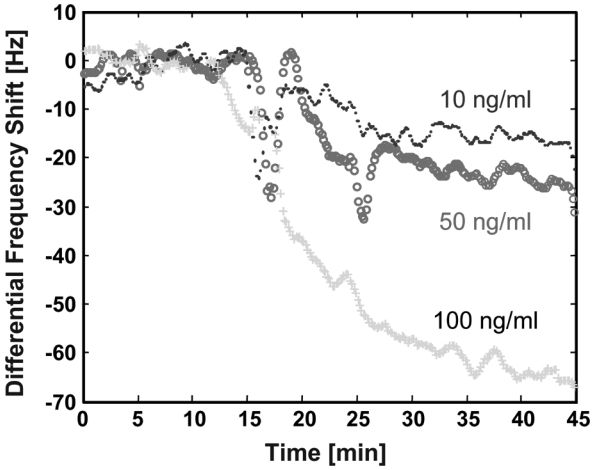

Fig. 18. Differential frequency response (antibody-coated versus uncoated cantilever) of the cantilever sensor system upon exposure to three different concentrations of prostate-specific antigen (PSA). The binding of PSA to PSA-antibodies immobilized on the cantilever via a protein-A layer was chosen as a model system. For details, see [20].

frequency data were filtered using MATLAB (Savitzky-Golay filter, window size 11). The signal distortion during the sample injection is most probably caused by the pumping. For clinical applications, the detection of PSA levels as low as 2 ng/ml in serum samples from real blood is necessary. The presented results are promising and indicate that this may be achieved with a fully integrated cantilever sensing system. It is estimated that for a clinical application the signal-to-noise ratio would have to be improved by at least a factor of 3.

VI. Conclusion

A monolithic cantilever-array-based mirosystem for bio-chemical sensing has been integrated using a standard 0.8 μm double-poly and double-metal CMOS process. In this paper, the design and implementation of the integrated circuitry and system have been presented along with first experimental results. The sensor system shows a frequency stability of better than 3 Hz in water corresponding to a limit of detection of about 30 pg mass loading. The system has been used for the detection of prostate-specific antigen on the cantilever surface at levels down to 10 ng/mL. It should be noted that the viscosity of the bio-fluid, or its possible changes must be monitored in biosensor applications. This can be done by using for instance an unspecific, i.e., non-functionalized, reference cantilever as done here.

Cantilevers are promising candidates for portable sensor devices due to their small footprint and low power consumption. The use in liquid phase, however, imposes special requirements on the design of the sensor and the integrated electronics, as well as the packaging. The fluid damping and the increased effective cantilever mass have to be dealt with in order to achieve stable cantilever oscillation. Furthermore, special care is needed to expose only the sensing area to the liquid while protecting and isolating the electrical connections and bond wires from the electrically conducting fluid.

Acknowledgment

The authors thank Prof. H. Baltes (Emeritus) for his interest in their work.

References

[1] D. Lange, "Cantilever-Based Microsystems for Gas Sensing and Atomic Force Microscopy," Ph.D dissertation, ETH Zurich, Zurich, Switzerland, 2000, Nr. 13984.

[2] G. H. Wu, R. H. Datar, K. M. Hansen, T. Thundat, R. J. Cote, and A. Majumdar, "Bioassay of prostate-specific antigen (PSA) using micro-cantilevers," *Nature Biotechnology*, vol. 19, pp. 856–860, 2001.

[3] C. Vancura, J. Lichtenberg, F. Josse, and A. Hierlemann, "Characterization of magnetically actuated resonant cantilevers in viscous fluids," *Appl. Phys. Lett.*, vol. 87, pp. 162510 1–162510 3, 2005.

[4] C. Vancura, Y. Li, K.-U. Kirstein, F. Josse, A. Hierlemann, and J. Lichtenberg, "Fully integrated CMOS resonant cantilever sensor for bio-chemical detection in liquid environments," in *Proc. TRANSDUCERS'05 (Seoul), Dig. Tech. Papers*, 2005, vol. 1, pp. 640–643.

[5] D. Lange, C. Hagleitner, C. Herzog, O. Brand, and H. Baltes, "Electromagnetic actuation and MOS-transistor sensing for CMOS-integrated micromechanical resonators," *Sensors & Actuators A*, vol. 103, pp. 150–155, 2003.

[6] C. Vancura, M. Ruegg, Y. Li, C. Hagleitner, and A. Hierlemann, "Magnetically actuated complementary metal oxide semiconductor resonant cantilever gas sensor system," *Anal. Chem.*, vol. 77, no. 9, pp. 2690–2699, May 2005.
[7] A. Hierlemann, *Integrated Chemical Microsensors in CMOS Technology*. Berlin, Germany: Springer-Verlag, 2005.
[8] E. Forsen, G. Abadal, S. Ghatnekar-Nilsson, J. Teva, J. Verd, R. Sandberg, W. Svendsen, F. Perez-Murano, J. Esteve, E. Figueras, F. Campabadal, L. Montelius, N. Barniol, and A. Boisen, "Ultrasensitive mass sensor fully integrated with complementary metal-oxide-semiconductor circuitry," *Appl. Phys. Lett.*, vol. 87, p. 43507, 2005.
[9] S. Ghatnekar-Nilsson, E. Forsen, G. Abadal, J. Verd, F. Campabadal, F. Perez-Murano, J. Esteve, N. Barniol, A. Boisen, and L. Montelius, "Resonators with integrated CMOS circuitry for mass sensing applications, fabricated by electron beam lithography," *Nanotechnology*, vol. 16, pp. 98–102, 2005.
[10] D. Jin, X. Li, H. Bao, Z. Zhang, Y. Wang, H. Yu, and G. Zuo, "Integrated cantilever sensors with a torsional resonance mode for ultra-resoluble on-the-spot bio/chemical detection," *Appl. Phys. Lett.*, vol. 90, no. 4, p. 041901, 2007.
[11] M. Sepaniak, P. Datskos, N. Lavrik, and C. Tipple, "Microcantilever transducers: A new approach to sensor technology," *Anal. Chem.*, vol. 74, pp. 568A–575A, 2002.
[12] F. Tian, K. M. Hansen, T. L. Ferrell, and T. Thundat, "Dynamic microcantilever sensors for discerning biomolecular interactions," *Anal. Chem.*, vol. 77, pp. 601–1606, 2005.
[13] E. Säckinger and W. Guggenbühl, "A versatile building block: The CMOS differential difference amplifier," *IEEE J. Solid-State Circuits*, vol. SC-22, no. 2, pp. 287–294, Apr. 1987.
[14] K. R. Laker and W. Sansen, *Design of Analog Integrated Circuits and Systems*. New York: McGraw-Hill, 1994.
[15] A. J. Gano and J. E. Franca, "Fully differential variable gain instrumentation amplifier based on a fully differential DDA topology," in *Proc. ICECS*, Pafos, Cyprus, 1999, vol. 2, pp. 781–784.
[16] S. Szezepansky, R. Schaumann, and P. Wu, "Linear transconductor based on cross-coupled CMOS pairs," *Electron. Lett.*, vol. 27, pp. 783–785, Apr. 1991.
[17] S. Szezepanski, A. Wyszynski, and R. Schaumann, "Highly linear voltage-controlled CMOS transconductors," *IEEE Trans. Circuits Syst. I, Fund. Theory Appl.*, vol. 40, no. 4, pp. 258–262, Apr. 1993.
[18] F. Krummenacher and N. Joehl, "A 4-MHz CMOS continuous-time filter with on-chip automatic tuning," *IEEE J. Solid-State Circuits*, vol. 23, no. 3, pp. 750–758, Mar. 1998.
[19] K. Kuo and A. Leuciuc, "A linear MOS transconductor using source degeneration and adaptive biasing," *IEEE Trans. Circuits Syst. II, Analog Digital Signal Process.*, vol. 48, no. 10, pp. 937–943, 2001.
[20] C. Vancura, Y. Li, J. Lichtenberg, K. U. Kirstein, A. Hierlemann, and F. Josse, "Liquid-phase chemical and biochemical detection using fully integrated magnetically actuated complementary metal oxide semiconductor resonant cantilever sensor systems," *Anal. Chem.*, vol. 79, pp. 1646–1654, 2007.

Yue Li received the M.S. and Ph.D. degrees in electrical engineering from ETH Zurich in 2001 and 2005, respectively.

She was a Circuit and System Designer in the Physical Electronics Laboratory (PEL) , Swiss Federal Institute of Technology (ETH), Zurich, Switzerland. Her research interests include analog integrated circuit design, and microsensor systems. Currently, she is working at CSEM, Zurich, Switzerland, on circuit design tasks for image sensor systems.

Cyril Vancura studied physics at the University of Kaiserslautern, Germany, and the Swiss Federal Institute of Technology (ETH), Zurich, Switzerland, where he received the diploma and Ph.D. degree from the Physical Electronics Laboratory, in 2001 and 2005, respectively.

Since 2006 he is working at the Research and Technology Center of Robert Bosch LLC, Palo Alto, CA. His research interests include microstructures for chemical and biological sensing and energy conversion devices.

Kay-Uwe Kirstein (M'03) received the diploma in electrical engineering from the University of Technology Hamburg-Harburg (TUHH), Germany, in 1997 and the Ph.D. degree from University Duisburg, Germany, in 2001. \

From 1997 to 2000, he was a Research Associate with the Fraunhofer Institut of Microelectronic Circuits and Systems, Dresden, Germany (now Fraunhofer Institute for Photonic Microsystems) where he was involved in the development of CMOS-based spatial light modulators. From 2000 to 2002, he worked in the analog circuit design group at Micronas GmbH, Freiburg, Germany. Afterwards, he has been team leader of the circuit design group at the Physical Electronics Laboratory, ETH, Zurich and has also been working on various IC-design projects in industry. Currently, he is part of the sensor development group at Uster Technologies, Uster, Switzerland. His research interests include analog and mixed-signal circuit design and behavioral modeling for CMOS-based microsystems.

Jan Lichtenberg received the M.S. degree in electrical and microengineering at the University of Bremen, Germany, in 1998. In 2002, he received the Ph.D. from the Institute of Microtechnology, University of Neuchâtel, Switzerland. His research with Prof. Nico F. de Rooij focused on microfluidic systems for chemical water analysis and medical diagnostics.

From 2002 until 2005, he was team leader of the Biosensor and Microfluidics Group at the Physical Electronics Laboratory of Prof. Henry Baltes at the ETH Zurich. Currently, he is Chief Technology Officer in the field of medical rehabilitation devices at Hocoma AG, Zurich, Switzerland. Besides his academic activities, he is also co-founder and a CEO for eight years of Advanced Micromachining Tools (AMMT GmbH), a leading supplier of equipment for MEMS fabrication.

Andreas Hierlemann (M'04) received the diploma in chemistry and the Ph.D. degree in physical chemistry from the University of Tübingen, Germany, in 1992 and 1996, respectively.

After working as a Postdoc at Texas A&M University, College Station, TX (1997), and Sandia National Laboratories, Albuquerque, NM (1998), he was appointed Associate Professor at the Physical Electronics Laboratory at ETH Zurich, Switzerland. In April 2008, he was promoted to Full Professor of Biosystems Engineering at the new Department of Biosystems Science and Engineering (BSSE) of ETH Zurich located in Basel, Switzerland. The focus of his research activities is on CMOS-based bio- and chemomicrosensors and on interfacing CMOS electronics with electrogenic cells.